Proceedings of the ASME 2011 International Mechanical Engineering Congress & Exposition
IMECE2011
November 11-17, 2011, Denver, Colorado, USA

IMECE2011-63861

PROPER ORTHOGONAL DECOMPOSITON ANALYSIS OF JAVA FLOWS FOR CROSS-FLOW CONDITIONS

Sertac Cadirci and **Hasan Gunes**
Department of Mechanical Engineering, Istanbul Technical University 34437 Gumussuyu
Istanbul, Turkey

ABSTRACT

Jet and Vortex Actuator (JaVA) is a zero-net-mass flux device for active flow control of boundary layers and transition. JaVA produces various jets which can be used to delay flow separation or to "steer" the boundary layer velocity profile. In this study, numerical simulations of JaVA-boundary layer interactions are analyzed using Proper Orthogonal Decomposition (POD). JaVA-induced flow regimes are governed by the plate width (***b***), the amplitude (***a***) and the operating frequency (***f***). In this study the frequency is changed between 2/3 Hz and 8/3 Hz keeping the plate width and the amplitude constant. A commercial finite-volume-based unsteady, laminar, incompressible Navier-Stokes solver has been used to study the flow fields generated by JaVA. Then, POD is applied to time dependent snapshots of velocity fields at each operating frequency. The POD modes revealed the behavior of the flat plate boundary layer under the effect of active flow control. Traveling modes can be captured in the successive modes for high frequencies.

***Keywords*:** Active flow control, Proper Orthogonal Decomposition (POD), Jet and Vortex Actuator, Boundary layer flow.

NOMENCLATURE

a	actuator plate amplitude [mm]
a_k	mode coefficient for velocity
A_{ki}	elements of k^{th} eigenvectors
b	plate width of the actuator [mm]
C_{ij}	correlation matrix
f	operating frequency of the actuator [Hz]
M	maximum snapshot (mode) number
N	snapshot number
r	cross flow parameter
Re_J	Reynolds number of the jet flow
S_a	scaled amplitude
t, T	time, period [s]
u,v	velocity components [cm/s]
U_0	free stream velocity [cm/s]
V	velocity vector
V_J	jet flow speed [cm/s]
w_n	narrow slot [mm]
w_w	wide slot [mm]
δ	displacement thickness [mm]
λ_i	eigenvalue
$\vec{\phi}_k$	eigenmodes (or eigenfunctions)
ν	kinematic viscosity [m^2/s]

INTRODUCTION

Jet and Vortex Actuator (JaVA) as an active flow control device can be applied to boundary layer flows to prevent or delay flow separation. The main principle of JaVA is based on increasing the momentum of the boundary layer flow by ejecting various jets or vortices. As a result, when applied to external flows on the airfoils, for instance; it can be used to control the flow similar to fixed vortex generators without inducing additional drag.

JaVA is classified as a zero-net-mass flux control device because it does not need any external fluid to operate. On the other hand, it is an active control device which can be adapted to various operating conditions just by altering governing parameters such as the amplitude, frequency or mean plate position. Due to its advantages active flow control is widely used against boundary layer flow separation at high Reynolds numbers (1). Other JaVA applications are mentioned in (2) where it is used during takeoff and landing of aircrafts.

It is emphasized in (3, 4) that JaVA may create efficient flight control systems where longer aircraft range might become possible at reduced cost. Recent studies of JaVA under water

have been carried out both experimentally and numerically (5-7).

The JaVA-induced flows in quiescent water have been investigated by extensive flow visualizations and then by Particle Image Velocimetry (PIV) measurements to understand the flow dynamics and to determine the effect of governing parameters on different flow types such as oblique jets, wall jets and vortices (5, 6 and 7). Supplementary experimental research is carried out in an open low-speed water channel with flow visualizations and PIV measurements where JaVA is mounted on a sufficiently long flat plate under water (8). Additionally the interaction of JaVA-induced regimes with the free stream velocity (channel flow) is simulated numerically for various operating conditions and it is shown that with increasing actuation effects (such as frequency, amplitude) the velocity profiles become "fuller" and thus can resist more to the flow separation (9).

In this study, we applied POD analysis to numerical simulations of JaVA flows in cross flow conditions. POD is a powerful approach to obtain low-dimensional dynamical models of thermo-fluid applications. It can be applied to time-dependent snapshots to extract coherent flow structures (modes). We refer to references (10, 11) for the basics of POD and its applications. As it is indicated in (12), the dynamical coherent structures of the turbulent boundary layer on a flat plate can be described by pairs of eigenfuncions. These eigenfunctions contain complete information on the spatial evaluation of the structures. POD is further applied to incompressible turbulent flow in a square duct (13) and it is shown that the extraction process reveals a gradual decrease of modal energies.

PROBLEM STATEMENT AND COMPUTATIONAL DOMAIN

JaVA is a rectangular cavity with an asymmetrically mounted plate on its top which moves vertically like a piston. The main parameters governing JaVA-induced flow regimes are the actuator plate's width ($\boldsymbol{b}$ = 25 mm), the amplitude ($\boldsymbol{a}$ = 1.5 mm) and the operating frequency ($\boldsymbol{f}$). The motion of the actuator plate is determined by the operating frequency varying between $\boldsymbol{f}$ = 2/3 Hz to 8/3 Hz and the amplitude. The actuator plate is flush-mounted due to the actuator box and its asymmetry engenders one narrow ($\boldsymbol{w_n}$= 0.3 mm) and one wide gap ($\boldsymbol{w_w}$ = 2.5 mm) between the plate and the box.

To characterize various flow regimes based on non-dimensional parameters, the jet Reynolds number and the scaled amplitude are derived from the dimensional parameters such as the amplitude, plate width and the frequency. The scaled amplitude is defined $\boldsymbol{S_a} = 2\pi\boldsymbol{a}/\boldsymbol{b}$, but it is constant as we keep the amplitude and the plate width constant at 1.5 mm and 25 mm respectively.

The JaVA-induced flows emerge out of the wide gap and are injected into the boundary layer, thus an average jet flow speed ($\boldsymbol{V_J}$) should be defined to obtain jet Reynolds number. Time-averaged integration of the jet velocity over a half period reveals the averaged jet velocity given in Eq. 1.

$$V_J = \frac{2}{T}\int_0^{T/2} v_j(t)\,dt = \frac{4abf}{w_w} \tag{1}$$

The jet Reynolds number ($\boldsymbol{Re_J}$) in Eq. 2 can be calculated using the averaged jet velocity and the wide slot gap. As all the parameters are kept constant except the frequency, the jet Reynolds number only varies with the frequency.

$$Re_J = \frac{V_J w_w}{\nu} = \frac{4abf}{\nu} \tag{2}$$

To express the effect of JaVA on the boundary layer, an additional so-called "cross flow parameter" given in Eq. 3 is needed. In simulations, the free stream velocity U_0 should be selected appropriately; otherwise JaVA-induced flow regimes can be suppressed by the incoming flow velocity.

$$r = \frac{V_J}{U_0} = \frac{4abf}{w_w U_0} \tag{3}$$

A commercial two dimensional finite-volume-based unsteady, laminar, incompressible Navier-Stokes solver has been used to study the flow fields generated by JaVA. The computational domain consists of a moving zone and the motion of the actuator plate is generated by a moving grid imposing appropriate boundary conditions with a User-Defined-Functions (UDF) as implemented in Fluent. Numerical simulations reveal the JaVA-boundary layer interaction for various frequencies (jet Reynolds numbers). The computational domain and the prescribed boundary conditions are shown in Fig.1.

The grid consisting of nearly 400000 cells, clustered in close vicinity of JaVA and the flat plate surface. After extensive grid checks, at least 20-80 cycles have been calculated depending on the frequency in order to reach the steady state in the flow domain. The periodic motion of the plate is a sinusoidal function depending on the frequency and the amplitude and this boundary condition is implemented as a UDF given in Eq. 4.

$$U_{plate} = 2\pi af\cos(2\pi ft) \tag{4}$$

Another UDF is implemented for the inlet boundary condition for which a fourth-order polynomial approximation for Blasius profile is used (Eq. 5) where the displacement thickness is denoted by $\boldsymbol{\delta}$. For simulations, the displacement thickness is calculated to be $\boldsymbol{\delta}$=21 mm (based on the experiments carried out in (8), free stream velocity U_0 =0.0838

m/s and the longitudinal distance from leading edge x = 1.53 m is taken).

$$\frac{u}{U_0} = \left[2\left(\frac{y}{\delta}\right) - 2\left(\frac{y}{\delta}\right)^2 + \left(\frac{y}{\delta}\right)^4 \right]; \ \delta = 5\sqrt{\frac{\nu x}{U_0}} \qquad (5)$$

Other feasible boundary conditions include outflow at the exit of the channel since there is no pressure gradient due to the flat plate and the free stream velocity at the upper boundary of the computational domain as the velocity profile does not change anymore far from the boundary layer edge. To obtain time-accurate solutions, the time step per iteration is taken Δt = 0.003125 s for all simulations.

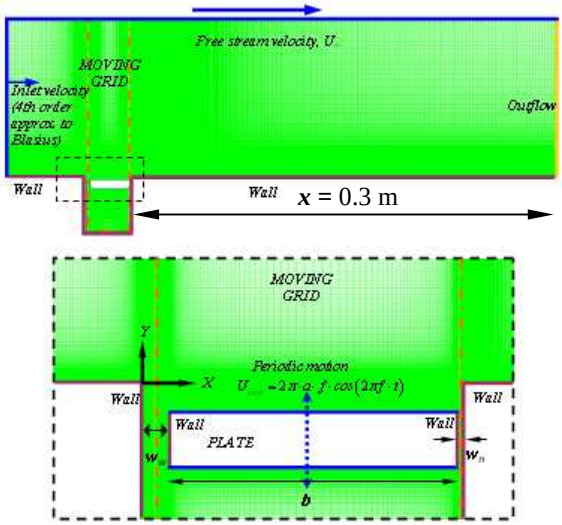

Figure 1: Computational domain and boundary conditions for JaVA in cross flow.

CFD RESULTS

One JaVA flow period consists of blowing and suction phases. The actuator plate moves up and down and its periodic motion is defined in Eq. 4. In a period as the plate moves into the cavity (blowing phase), jet-like vortex pairs are ejected out of the wide slot (w_w). When the plate moves in the opposite direction (out of the cavity), the fluid is sucked from the surrounding medium into cavity (suction phase). Fig. 2 shows the phase-averaged flow fields for f = 8/3 Hz.

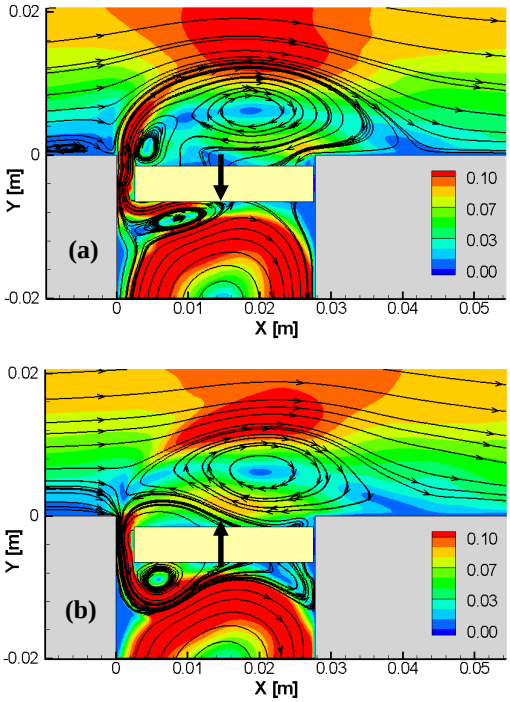

Figure 2: Phase averaged flow fields in m/s for (a) blowing, (b) suction – (f = 8/3 Hz, Re_J = 400, r = 1.92).

While figure 2 shows the detailed behaviour of the suction and blowing phases, the boundary layer velocity profiles extracted from different locations in the time-averaged flow fields downstream of JaVA reveal the effect of the actuation on the boundary layer. With increasing frequency or cross flow parameter, the ejected vortices energize the boundary layer and help delay or resist boundary layer separation and yield "fuller" boundary layer velocity profiles compared to the uncontrolled case (f = 0) as Fig. 3 indicates.

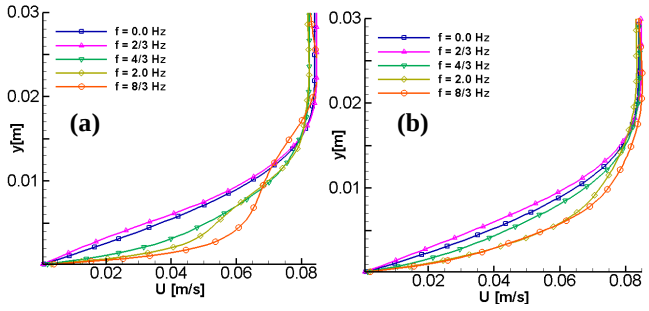

Figure 3: Time-averaged velocity profiles at (a) x = 0.1 m, (b) x = 0.3 m (exit) downstream of JaVA.

PROPER ORTHOGONAL DECOMPOSITION

POD provides a basis for the modal decomposition of a system of functions, usually data obtained from numerical simulations or experimental measurements. The basis functions

retrieved are called proper orthogonal modes. It provides an efficient way of capturing the dominant components of a multidimensional system and representing it to the desired precision by using the relevant set of modes. The method can be applied to experimental as well as complex numerical solutions and in many diverse fields as given in (14, 15).

The "snapshot version" of POD introduced in (16) is an efficient implementation for "time-dependent" flow fields. In this study we employ snapshot version of POD as the database consists of time dependent snapshots of numerically obtained two dimensional velocity fields. For an operating condition, one period consisting of at least 200 instantaneous snapshots is stored and then this numerical database is analyzed by POD to extract coherent flow structures that supply valuable information about flow dynamics. The POD modes or "eigenfunctions" for velocity are calculated as

$$\vec{\phi}_k(x,y) = \sum_{i=1}^{M} A_{ki}\vec{V}(x,y,t_i)\,. \tag{6}$$

In Eq.6, $\boldsymbol{M}$ is the total number of snapshots, $\vec{V}(x,y,t_i)$ is the i^{th} velocity field and $\boldsymbol{A_{ki}}$ are the elements of k^{th} eigenvectors in the correlation matrix $\boldsymbol{C_{ij}}$. The elements of the correlation matrix are calculated as

$$C_{ij} = \frac{1}{M}\iint \vec{V}(x,y,t_i)\vec{V}(x,y,t_j)dxdy\,. \tag{7}$$

The correlation matrix is symmetric and positive-definite therefore its eigenvalues are real positive numbers. The eigenvalues can be sorted in descending order as in Eq. 8. The sum of all the eigenvalues is the total flow energy and each POD mode is represented by the magnitude of the corresponding eigenvalue.

$$\lambda_1 \geq \lambda_2 \geq \lambda_3 \geq .....\geq \lambda_M \tag{8}$$

The velocity field can be expanded in a series in Eq. 9 where $\boldsymbol{N}$ (usually $\boldsymbol{N}<<\boldsymbol{M}$) is the number of most energetic modes. In this formulation $\boldsymbol{a_k}$ is the time varying expansion coefficient and the POD eigenfunctions are calculated using Eq. 10. Together with Eq. 9, it is called reconstruction formula.

$$\vec{V}(x,y,t) = \sum_{k=1}^{N} a_k(t)\vec{\phi}_k(x,y) \tag{9}$$

$$a_k(t) = \iint \vec{V}(x,y,t)\vec{\phi}_k(x,y)dxdy \qquad k = 1,2,\ldots N \tag{10}$$

POD MODES

The POD modes reveal the periodic behavior of the flat plate boundary layer under the effect of active flow control. Especially, the traveling modes can be captured in the successive modes for high frequencies.

Fig. 4 and 5 show the first 10 POD modes for $\boldsymbol{u}$ and $\boldsymbol{v}$-velocity components at $\boldsymbol{f}$ = 2 Hz ($\boldsymbol{Re_J}$ = 300, $\boldsymbol{r}$ = 1.44) respectively. The most energetic eigenfunctions ($\boldsymbol{M}$ = 1, 2) contain the large scale features of each field. Higher modes ($\boldsymbol{M}$ = 9, 10) have a lower energy level and capture the small scale features of the fields. The maximum number of snapshots is 200 in this case, but the 10 most energetic eigenfunctions are represented.

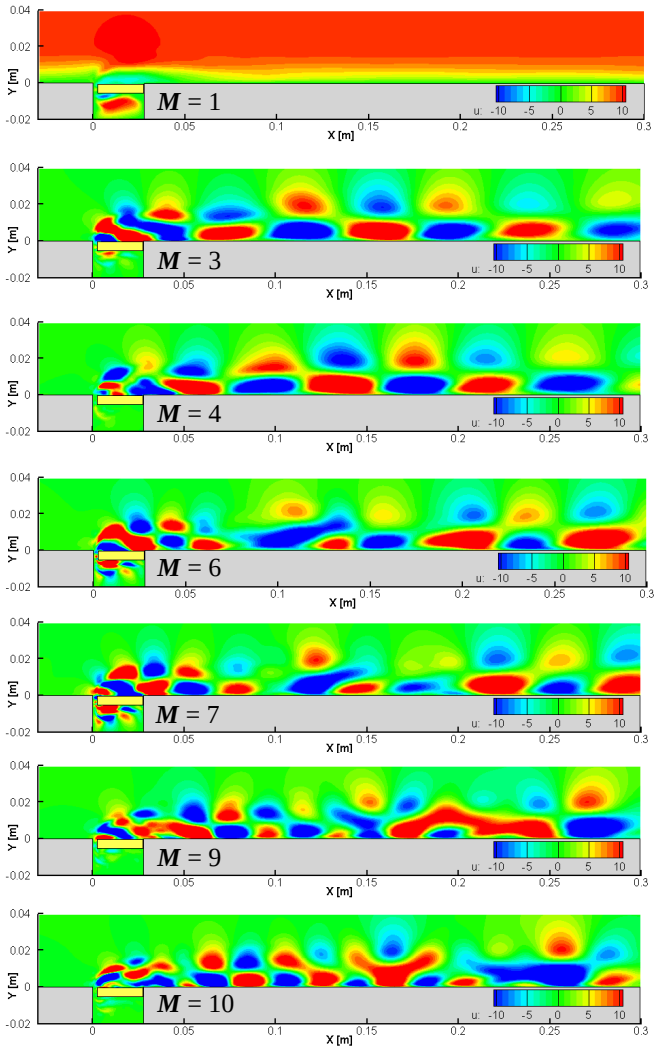

Figure 4: The $\boldsymbol{u}$-velocity field POD modes (the mode number is listed in decreasing energy)-$\boldsymbol{Re_J}$ = 300.

The first mode ($\boldsymbol{M}$ = 1) contains the highest energy and it represents the "mean" flow field: the first mode of the $\boldsymbol{u}$-velocity distribution is equivalent to the time-averaged channel flow as the free stream velocity is in x-direction; and the first mode of the $\boldsymbol{v}$-velocity distribution does not indicate any significant flow field except JaVA-induced jet emerging out of

the wide slot and the circulation in the cavity. The eigenfunctions for the ***v***-velocity component within each pair are phase shifted in the flow direction of the channel ($\phi_3 - \phi_4$, $\phi_6 - \phi_7$ and $\phi_9 - \phi_{10}$).

A general remark derived from the eigenmodes of all the cross flow parameters is that as the jet Reynolds number increases (Re_J = 300 and 400), the small scale features gain in energy and they become more visible. With increasing jet Reynolds number, the small scale features become bigger in size and stretch through the flow region. As the mode number increases, the energy content drops considerably and detailed structures about the flow fields can be observed (see Fig. 5).

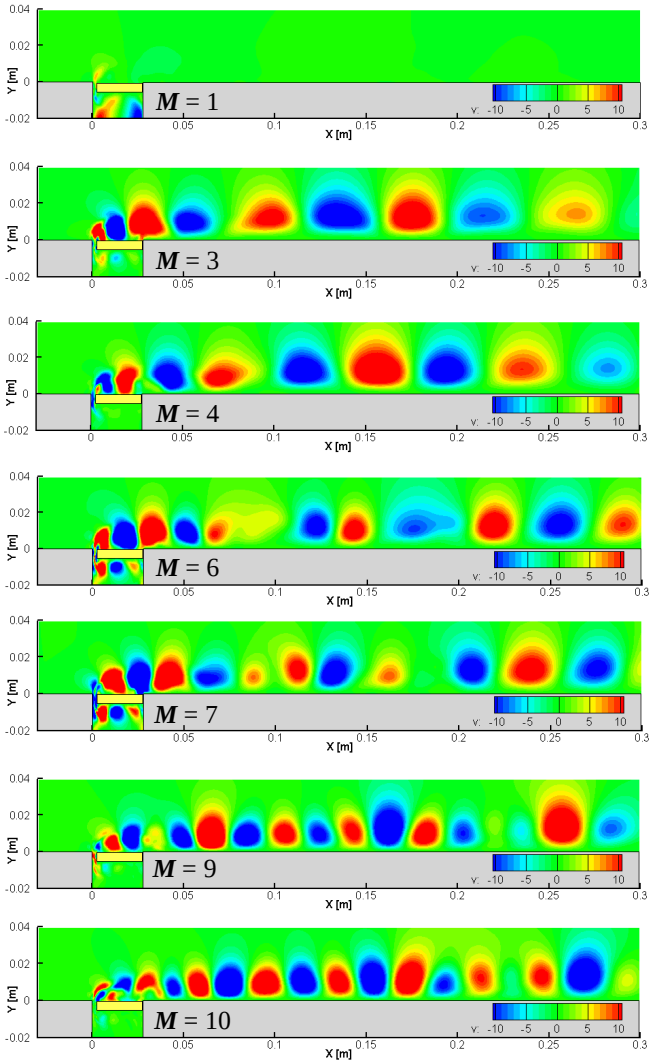

Figure 5: The ***v***-velocity field POD modes (the mode number is listed in decreasing energy)-Re_J = 300.

RECONSTRUCTION OF JAVA FLOW

Reconstruction is carried out using Eqs. (9) and (10) to recreate an arbitrary flow field in the database. If the flow field to be reconstructed already exists in the database, it is called "on-design reconstruction". If it is aimed to obtain a flow field that is not included in the database, it is called "off-design reconstruction". Off-design reconstruction is often utilized to predict a flow field with off-design jet Reynolds number. As we applied POD to datasets consisting of time-dependent instantaneous snapshots for a single jet Reynolds number, it makes more sense to reconstruct a design point. Note that the reconstruction process is only possible using time-dependent expansion coefficients (a_k). The reliability and robustness of the reconstruction referred to a design point improves with the increasing modes number as Fig. 6 shows the predicted flow fields for Re_J = 300 and 400.

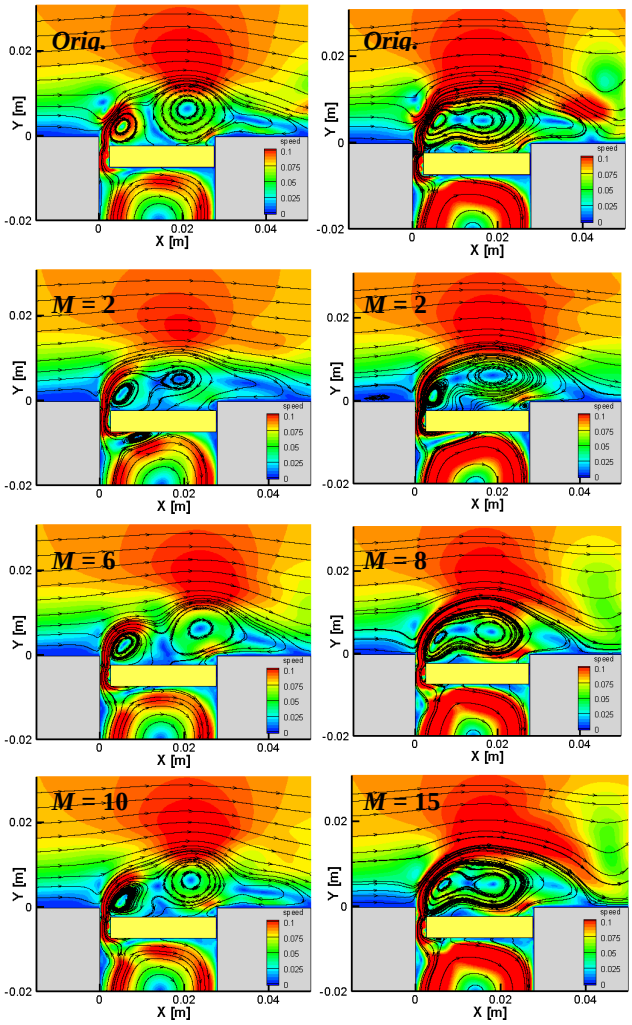

Figure 6: The reconstruction of the flow fields (left column: Re_J = 300 and right column: Re_J = 400).

Figure 7 shows the cumulative eigenvalues (λ_i) for each operating condition. The cumulative eigenvalus are obtained by the summation of the "normalized eigenvalus" where the first

mode is purposely left out of the list as it contains the highest energy level representing the mean flow. To reconstruct an arbitrary snapshot with a very high accuracy, "18" modes are required since the respective contribution of the cumulative eigenvalues to the total flow energy is more than 90% at this level for Re_J = 300. On the other hand, this percentage can only be captured for Re_J = 400, if "24" modes are selected for the reconstruction. However, only "10" most energetic modes are assumed to be sufficient to recreate the original flow domain for Re_J = 300 and "15" modes are required for an accurate reconstruction if the jet Reynolds number increases to 400. This can be explained by the eigenvalues and their respective contributions to the total flow energy as mentioned. In addition to that, the maximum number of instantaneous snapshots for Re_J = 400 is M = 240 where the modes' number should be higher for an accurate reconstruction compared to other cases.

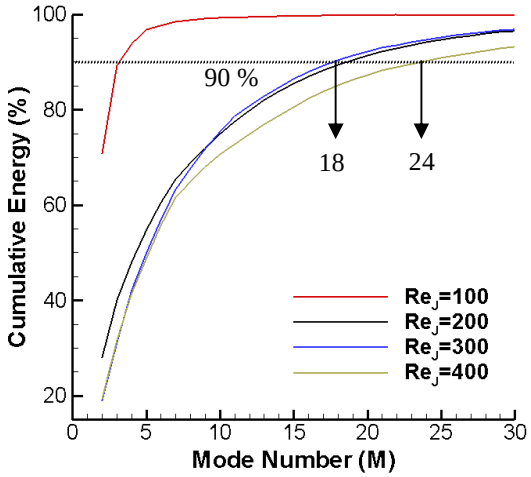

Figure 7: The "30" largest cumulative eigenvalues (λ_i) and their respective contributions to the total flow energy.

Figure 8a shows the variation of expansion coefficients (a_2) with respect to mode number for the investigated cases. These are the temporal expansion coefficients obtained by direct projection of the input velocity data on the POD modes (17). It should be noted that the amplitudes of the expansion coefficient (a_2) increase as the jet Reynolds number increases.

Other expansion coefficients corresponding to a pair (a_3-a_4 a_6-a_7 and a_9-a_{10}) are phase shifted as the plots for Re_J = 300 indicate in Fig. 8b, c and d. The product of $a_i\phi_i$ (no summation) represents a standing wave. It is noted in the literature that when two standing waves are out of a phase by a quarter of period in time and space, a "travelling wave" is formed (17).

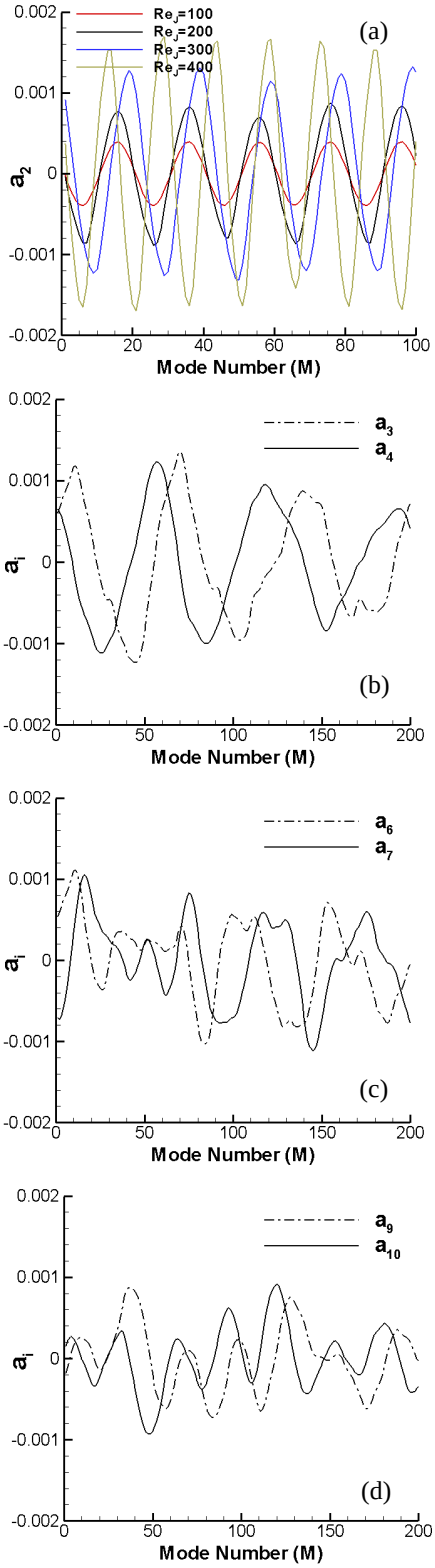

Figure 8: Variation of expansion coefficients: (a) a_2 for various Re_J, (b) a_3-a_4 , (c) a_6-a_7 and (d) a_9-a_{10}.

The *rms* (root mean square) errors are tabulated in Table 1. The rms error drops with increasing mode number for both velocity components. This leads to the idea that the inclusion of the first "10" POD modes is sufficient to reconstruct an ensemble member of the dataset.

Table 1: The rms-errors for design reconstruction.

M	*rms (u)*			
	Re_J = 100 r = 0.48	Re_J = 200 r = 0.96	Re_J = 300 r = 1.44	Re_J = 400 r = 1.96
2	$5.91\ 10^{-4}$	$5.41\ 10^{-3}$	$9.56\ 10^{-3}$	1.3110^{-2}
4	$5{,}16\ 10^{-4}$	$4.07\ 10^{-3}$	$8.52\ 10^{-3}$	8.9010^{-3}
6	$2{,}94\ 10^{-4}$	$3.29\ 10^{-3}$	$6.58\ 10^{-3}$	$8.43\ 10^{-3}$
8	$2{,}68\ 10^{-4}$	$3.18\ 10^{-3}$	$5.70\ 10^{-3}$	$6.77\ 10^{-3}$
10	$2{,}68\ 10^{-4}$	$2.76\ 10^{-3}$	$4.56\ 10^{-3}$	$5.80\ 10^{-3}$

M	*rms (v)*			
	Re_J = 100 r = 0.48	Re_J = 200 r = 0.96	Re_J = 300 r = 1.44	Re_J = 400 r = 1.96
2	$5.59\ 10^{-4}$	$4.68\ 10^{-3}$	$8.19\ 10^{-3}$	$1.21\ 10^{-2}$
4	$4.69\ 10^{-4}$	$3.37\ 10^{-3}$	$7.70\ 10^{-3}$	$9.31\ 10^{-3}$
6	$2.32\ 10^{-4}$	$3.01\ 10^{-3}$	$6.44\ 10^{-3}$	$8.84\ 10^{-3}$
8	$1.97\ 10^{-4}$	$2.94\ 10^{-3}$	$5.46\ 10^{-3}$	$7.24\ 10^{-3}$
10	$1.12\ 10^{-4}$	$2.73\ 10^{-3}$	$4.47\ 10^{-3}$	$5.96\ 10^{-3}$

CONCLUSION

In this study the POD analysis of Jet and Vortex Actuator (JaVA)-induced flow regimes for cross flow conditions is carried out to capture the travelling waves in the modes and reconstruct an instantaneous snapshot in the database. The numerical database consists of time-dependent snapshots (200 or 240) obtained by solving a two-dimensional Navier-Stokes equations on a flat plate under the effect of actuation at various operating frequencies. A moving grid in the computational domain with appropriately selected User-Defined-Functions as boundary conditions are implemented. The solution is carried out using a commercial laminar-incompressible finite-volume based flow solver and it is shown that for the same operating conditions including the free stream velocity, a robust boundary layer profile that resists flow separation can be achieved if the jet Reynolds number or "cross flow parameter" is increased.

The datasets ($\boldsymbol{Re_J}$ = 100, 200, 300 and 400) are evaluated by POD separately. The spatiotemporal coherent structures are identified as travelling waves that depend on the jet Reynolds number. As the jet Reynolds number increases, high order POD modes gain energy and their relative contribution to the total fluctuating kinetic energy increases. The energy gain of higher modes affects the POD modes resulting in larger and stretched structures, thus phase shifting can be observed clearly. The expansion coefficients justify that the modes (e.g., 3-4, 6-7 and 9-10) are phase-shifted. The cumulative energy content reaches almost 95 % if the first "30" POD modes are taken into account. Additionally, an arbitrary snapshot in the dataset can be reconstructed (on-design reconstruction). As expected, the rms-error drops with increasing mode number.

POD analysis shows that the travelling waves in unsteady flow fields can be captured for JaVA flows for cross-flow conditions.

REFERENCES

[1] Seifert, A., and Pack, L., "Oscillatory Control of Separation at High Reynolds Numbers," *36th Aerospace Sciences Meeting and Exhibit*, AIAA 98-0214, Reno, Nevada, 1998.

[2] Johnston, J. P., and Nishi, M., "Vortex Generator Jets-A Means for Separation Control," *AIAA Journal*, Vol. 28, No. 6, 1990, pp. 989-994.

[3] Lachowicz, J. T., Yao C., and Wlezien, R. W., "Physical Analysis and Scaling of a Jet and Vortex Actuator," *Proceedings of the 3rd ASME/JSME Joint Fluids Engineering Conference*, FEDSM'99-6921, ASME, San Francisco, California, 1999.

[4] Lachowicz, J. T., Yao, C., and Wlezien, R. W., "Flow Field Characterization of a Jet and Vortex Actuator," *Experiments in Fluids*, Vol. 27, 1999, pp. 12-20.

[5] Gunes, H., Cadirci, S., and Rist, U., "An Experimental Investigation of Jet and Vortex Actuator for Active Flow Control," AIAA Paper No. 3761, *4th Flow Control Conference and Exhibit*, Seattle, Washington, 2008.

[6] Gunes, H., Cadirci, S., Baldani, F., Peters, B., and Rist, U., "Temporal Analysis of Jet and Vortex Actuator (JaVA)-induced Flows," *International Conference on Jets, Wakes and Separated Flows*, ICJWSF, Berlin, Germany, 2008.

[7] Gunes, H., Cadirci, S., and Rist, U., "Experimental Investigation of Jet and Vortex Actuator Using Particle Image Velocimetry," *ASME International Mechanical Engineering Congress & Exposition*, ASME-IMECE2009-11451, Orlando, Florida, 2009.

[8] Cadirci, S., "Experimental and Numerical Investigation of a Jet and Vortex Actuator for Active Flow Control", *Ph.D. Thesis*, Istanbul Technical University- Institute of Science and Technology, October 2010.

[9] Cadirci, S., Gunes, H., Rist, U., "Numerical Investigation of Jet and Vortex Actuator (JaVA) for Active Flow Control" AIAA- *5th Flow Control Conference*, Chicago, 2010.

[10] Lumley, J. L., 1967 "*The Structure of Inhomogeneous Turbulence. In Atmospheric Turbulence and Wave*

Propagation" A. M. Yaglom, V. I. Tatarski, Moscow, pp. 166-178.

[11] Berkooz, G., Holmes, P., and Lumley, J. L., 1993, "The Proper Orthogonal Decomposition in the Analysis of Turbulent Flows" *Ann. Rev. Fluid Mech*. **25**, pp. 539-575.

[12] Rempfer, D., Fasel F.H., 1993, "Evaluation of three-dimensional coherent structures in a flat-plate boundary layer", Journal of Fluid Mechanics 260, p. 351-375- *Cambridge University Press.*

[13] Reichert, R.S., Hatay F.F., Biringen S. and Huser A., 1994, "Proper orthogonal decomposition applied to turbulent flow in a square duct", *Physics of Fluids* 6 (9).

[14] Everson, R. and Sirovich, L., 1995, "The Karhunen-Loeve Transform of Incomplete Data" *J. Optical Soc. of America*, **12** (8).

[15] Tan, B.T., Willcox, K., Damodaran, M., 2003, "Applications of Proper Orthogonal Decomposition for Inviscid Transonic Aerodynamics" 21st *Applied Aerodynamics Conference*, AIAA Paper No. 4213.

[16] Sirovich, L., 1987, "Turbulence and the Dynamics of Coherent Structures" *Applied Mathematics* **45** (561).

[17] Sahan, R. A., Liakopoulos, A. and Gunes, H., 1997, "Reduced Dynamical Models of Non Isothermal Grooved-Channel Flow" *Physics of Fluids*, **9** (3).